J of Nuclear Medicine Technology, first published online April 19, 2022 as doi:10.2967/jnmt.121.263534

Biology of Cancer and PET Imaging: Pictorial Review

Ismet Sarikaya

Kuwait University Faculty of Medicine and Mubarak Al-Kabeer Hospital Department of Nuclear Medicine, Kuwait.

Correspondence Address:

Ismet Sarikaya, MD, ABNM
Department of Nuclear Medicine
Faculty of Medicine, Kuwait University
PO Box 24923
Safat, Kuwait 13110
Phone: (965) 2539592 / 6414
Fax: (965) 25338936
Email: isarikaya99@yahoo.com

Running title: Cancer Biology and PET

Abstract

Development and spread of cancer is a multi-step and complex process which involves number of alterations, interactions and molecular networks. PET imaging is closely related with cancer biology and pathology as it uses various radiotracers targeting biological and pathological changes in cancer cells and tumor microenvironment. In this review article, biology of development and spread of cancer and role of PET imaging in Oncology was summarized and supported with various PET images demonstrating cancer spread patterns.

Key words: Cancer, spread, invasion, metastasis, PET, FDG

Introduction

Approximately 17 million new cancer cases were diagnosed and 10 million people died because of cancer in 2018 (1). The 3 most common sites of new cancers were lung (1,368,500), prostate (1,276,100) and colorectal region (1,026,200) in men and breast (2,088,800), colorectal region (823,300) and lung (725,400) in women in 2018 (1). Each year, approximately 400,000 children (0-19 years old) are diagnosed with cancer (2).

Development and spread of cancer is a multistep and complex process which involves number of alterations in the cell, interactions between cancer cells and multiple cell types in the local and distant environments and multiple-molecular networks. Carcinogenesis is a multistep process with initiation, promotion, and progression phases and requires multiple mutations over the life time. Positron Emission Tomography/Computed Tomography (PET/CT) has been widely used for cancer imaging in the last 20 years. In this review article, biology of cancer (development of cancer, modes and mechanisms of cancer spread) and current role of PET imaging in oncology will be summarized and supported with PET images of various cancer spread patterns.

Biology of Development, Invasion and Metastasis of Cancer

Carcinogenesis is the development of cancer cells from a normal cell. In normal cells, the cell cycle is regulated by positive and negative feedback signals. Cell cycle has multiple phases which includes quiescent/resting phase (G0), interphase (G1, S, and G2 phases), mitotic phase (M), programed cell death phase with checkpoints in interphase and mitosis (3,4). p53 is one of the main control proteins which suppresses cell cycle progression in DNA-damaged cells and also aids DNA repair. A number of genetic alterations occur in cancer cells to overcome the regulated cell growth. In most of the malignancies, the G1/S checkpoint is involved (3).

Acquired mutations are the most common cause of cancer which can occur due to various

factors such as tobacco use, radiation, viruses, chemicals, chronic inflammation, aging, and environment. Germline mutations are the cause in about 5% to 20% of malignancies (5). The carcinogenic process involves the alteration/mutation in cancer genes such as activation of oncogenes (e.g HER2, RAS family, and RAF), inactivation of tumor suppressors (e.g. BRCA1, BRCA2, and p53), evasion of apoptosis genes, and defect in DNA repair genes. In up to 60% of cancers there is mutation in p53 gene and in 30% of the cancers there is mutation in RAS/RAF/MEK/ERK pathway (4).

Neoplasms are derived from a single clone of cells which grow in an uncoordinated manner. The biologic characteristics and hallmarks of cancer cells include ability for a cancer to generate mitogenic signals, evading/resisting immune killing, resisting growth suppression, genetic instability, evading apoptosis, acquiring unregulated sustained proliferation (immortality), angiogenesis, altered metabolism, inflammation, tumor heterogeneity, tissue invasion and metastasis (6-8). Cancer cells within the tumor are morphologically, biochemically, and genetically heterogeneous. The most definite hallmark of the cancer is the subsets of the neoplastic cells to escape through the basement membrane and penetrate into stroma (6).

Re-modelling in cellular junctions, interaction between the cells and the extracellular matrix through cell adhesion molecules (e.g. integrins, selectins, cadherins, Ig superfamily, CD44), focal adhesions, and other substances (e.g. matrix metalloproteinases, EPLIN) are involved in various steps of cancer progression, cell motility and migration (9). After cancer cells escape the basement membrane, tumor invades/penetrates the surrounding tissues and metastasize to distant organs. Various promoter genes are implicated in invasion and metastasis. Detachment and escape of cells from the primary tumor mimics the developmental process known as epithelial mesenchymal transition (9,10). Degradative enzymes produced by the tumor or tumor–associated

cells remodel the extracellular matrices and facilitate tumor cell invasion and progression. Tumor microenvironment consists of tumor cells and various tumor-associated host cells which makes about half of the total number of cells in malignant tumors which play critical role in cancer initiation, progression and metastasis (particularly cancer associated fibroblasts expressing fibroblast activation protein-α and immune cells) (6,11). Tumor cells can disseminate as individual cells or move as collective groups (plasticity of tumor cell movement) (12,13). Tumor cells eventually migrate towards to transportation compartments such as blood vessel, lymphatic channels, or coelomic cavities with interconnectivity between transit compartments.. Most of the distant metastases are hematogenous. Initially, tumor receives blood supply from the vessels in the new soil or form tubes to anastomose with the existing capillaries, but later angiogenesis is induced for further growth of the tumor.

Growth of new blood and lymphatic vessels occur in the primary and metastatic tumor. Angiogenesis occur via various mechanisms such as formation and outgrowth of sprouts, formation of new vasculature from existing vessels, recruitment of circulating endothelial progenitor cells, vascular mimicry, and trans-differentiation of cancer stem cells (14). Lymphatic enlargement and lymphangiogenesis via growth factors produced by tumor and tumor microenvironment cells occur in the primary tumor and sentinel lymph nodes (15).

Summary of PET Imaging in Oncology

PET imaging is closely related with cancer biology and pathology as it uses various radiotracers to detect cancer based on biological and pathological changes in cancer cells and tumor microenvironment. PET/CT has been widely used for cancer imaging since early 2000. PET/magnetic resonance imaging (MR) is also available in the last 10 years. Recently, total body

PET/CT cameras have been introduced which allow imaging the entire body simultaneously within few minutes (16).

PET is used for initial staging, assessing response to various treatments, detecting recurrences, differentiating benign from malignant lesions, guiding biopsies, planning radiotherapy, selecting patients for treatments, searching for primary tumor in cases with primary unknown metastases and paraneoplastic syndromes, predicting tumor grade, aggressiveness, heterogeneity, prognosis and survival. There are various PET radiotracers which can detect cancer cells based on increased metabolism (e.g. glucose, fatty acids, and lactate), synthesis of proteins, DNA, and cell membrane as markers of cellular proliferation, and expression of various receptors, enzymes and tumor-associated/specific antigens. Table 1 demonstrates the common and uncommon PET radiotracers for cancer imaging.

18Fluorine (18F)-fluorodeoxyglucose (FDG) is the most commonly used PET radiotracer to image cancer. Cancer cells mainly use glucose for their energy needs (aerobic glycolysis, Warburg effect) with accelerated glucose metabolism, increased rate of glucose transport and glycolysis, over expression of glucose transporters and hexokinase enzyme. Tumor microenvironment also effect glucose metabolism of cancer cells. Breast cancer, particularly invasive and inflammatory, is among the most common indications of FDG PET imaging mainly for staging (particularly stage 3 and 4), assessing response to treatments and detecting recurrences (17,18). FDG PET is indicated for initial staging of all cases of non-small cell lung cancer and initial staging of pure and combined small cell lung cancer (17). FDG PET is used for differential diagnosis of solid solitary pulmonary nodules that are greater than 8 mm in size (19). In multiple myeloma, FDG PET helps to distinguish inactive from active disease, to detect extramedullary disease, to monitor effect of treatments, and to determine progression from smouldering myeloma.

FDG PET is standard for lymphoma staging (Hodgkin and various Non-Hodgkin lymphomas such as such as diffuse large B-cell, follicular, MALT and mantle cell subtypes) and end of treatment response assessment. In head and neck, FDG PET is indicated in detecting occult primary and recommended for initial staging and assessing response to treatment. FDG PET is recommended in anaplastic thyroid cancer and in papillary, follicular and hurthle cell carcinomas if stimulated Tg > 2-5 ng/mL and I-131 imaging negative (17). High grade gliomas, particularly Glioblastoma multiforme, are usually FDG avid. FDG PET helps to differentiate high from low grade gliomas, determine extent of tumor for treatment planning, detect recurrences and guide biopsies. Most of the soft tissue and bone sarcomas are highly FDG avid. FDG PET helps staging and assessing response to treatment with thyrosine kinase inhibitors in gastrointestinal stromal tumors. Most paragangliomas are FDG avid, particularly cases with succinate dehydrogenase-B (SDHB) mutation (20). Malignant melanoma is highly FDG avid. FDG PET is recommended for initial staging of stage 3 and 4 melanoma and can be used in earlier stages if patients have clinical signs and symptoms (17). FDG PET can also demonstrate cancer related complications such as tumor thrombus and emboli, fracture, and inflammatory changes.

Radiolabeled ligands of prostate specific membrane antigen (PSMA), most notably 68Gallium (68Ga)-PSMA-11, are used for initial staging of high-risk prostate cancer and detecting recurrences with higher efficiency than Choline PET and Fluciclovine PET at low PSA levels (21,22). PSMA PET is also used for selecting patients and assessing response to treatment for PSMA targeted radionuclide treatments. Somatostatin receptor (SSR) PET imaging has high sensitivity in detecting various well-differentiated NETs (e.g. carcinoid) expressing high SSRs (particularly SSR2, 3 and 5 subtypes) and certain types of paragangliomas (20). 18F-fluoroestradiol (FES) PET helps to determine estrogen receptor status of the breast and ovarian

cancers. Radiolabeled amino acid tracers such as C-11 methionine, F18-FDOPA, and F18-fluoroethyltyrosine have high sensitivity in detecting primary and recurrent Glioblastoma multiforme. F18-thymidine have been studied grading, assessing tumor heterogeneity and detecting recurrences in gliomas. FDOPA is also useful for detecting medullary thyroid carcinomas and SDHB-negative paragangliomas (23). Various hypoxia imaging radiotracers help to identify tumor hypoxia which is important for radiotherapy planning, assessing tumor heterogeneity, and selecting patients for hypoxia-targeted therapeutics. Radiolabeled fibroblast activation protein inhibitors show uptake in various cancers with promising results (24). Immuno-PET imaging with radiolabeled antibodies against tumor-associated/specific antigens have been studied in detecting cancer and assessing response to treatment.

Targeted radionuclide treatment of cancer using various beta and alpha particle emitters is a rapidly evolving area. By showing the presence, extent and intensity of the target expression in the tumor, theranostic PET imaging helps selecting patients for targeted radionuclide treatment, determining the treatment dose and assessing response to treatment.

Precision medicine is the selection of the right treatment using various diagnostic tests (molecular, imaging) and analytics for a group of individuals with certain characteristics, whereas personalized medicine is to choose the right treatment for an individual patient. PET offers various biomarkers to image hypoxia, angiogenesis, apoptosis, metabolism, receptor expression etc. to determine tumor characteristics and heterogeneity which help to choose the right treatment, and identify resistance to therapies with early therapy response assessment.

18F and 68Ga are the most commonly used PET radionuclides for radiolabeling molecules for cancer imaging. The other PET radionuclides, such as Carbon-11 and other radiometals (e.g. Zirconium-89, Copper-64, Yttrium-86, radioisotopes of Scandium and Terbium) have also been

studied to label various molecules. Radiometals are mainly used to label peptides, proteins, antibodies and ligands due to their longer half-lives and longer circulation of such molecules. Longer half-life is also an advantage in regard to shipment.

PET images are supported by various parameters to better assess radiotracer uptake and distribution in the tumor such as standardized uptake value (SUV), metabolically active tumor volume (MTV), global metabolic tumor volume (GMV), total lesion glycolysis (TLG), dual or multiple time-point PET imaging with retention index, dynamic PET imaging, and parametric PET imaging with kinetic modelling and quantitative analysis (25). Various PET response criteria are used to better assess response to chemotherapy, radiotherapy, and treatment with immune checkpoint inhibitors (26).

Figure 1 demonstrates development of a cancer on serial PET images. Supplemental Figure 1 demonstrates PET image of local cancer invasion.

PET imaging has a well-established role in cancer management but it has certain limitations such as detecting small tumor foci, quantification of radiotracer uptake and tumor volume and non-specificity of radiotracers. The spatial resolution of PET has been increasing (in the range of 5-8 mm for the trunk and 3-5 mm for the brain and extremities), but smaller and microscopic/sub-milimetric foci cannot be detected. Ultra-high resolution brain PET scanners are being developed which may detect brain lesions 1.6-1.8 mm in size (27). Current PET radiotracers are not purely cancer specific and may show uptake in benign lesions, normal tissues, and inflammation following treatments (28). Low grade and well-differentiated tumors show low glucose metabolism or certain tumors may use other fuels for their energy need which reduces sensitivity of FDG PET in such tumors. Tumor cells may lack or lose antigen/receptor expression which limits the efficiency of PET radiotracers targeting such expressions. Certain PET

radiotracers that are relatively more specific for a histological type of cancer may also show uptake in other cancer types, such as PSMA ligands. PET parameters, particularly SUV is effected by various factors, most notably blood glucose and body mass index (25, 29). SUV normalized by lean body mass (SUL) or tumor to reference SUV ratios can be used when assessing response to treatments in obese and overweight patients (30,31). Certain medications can effect uptake and distribution of radiotracers and should be stopped prior to PET studies. Calculation of local or global tumor volume with threshold and algorithm based methods has certain limitations with over- or underestimation of the tumor volume (32). Artifacts can be seen on PET/CT images due to motion, arm positioning, dense material or objects (33-35). Various attempts, reconstruction techniques and softwares are available to overcome some of these artifacts.

Modes of Metastatic Spread of Cancer and PET Images

Metastases through Lymphatic System

Cancer cells enter or invade the lymphatic vessels and migrate to tumor-draining sentinel lymph node. High interstitial fluid pressure in the tumor facilitate the entry of cancer cells into lymphatic vessels (36). Tumor cells and cells in tumor microenvironment produce growth factors that promote peri-tumoral lymphangiogenesis which provides tumor cells access to more lymphatic vessels. Cancer cells can also move toward and invade lymphatic vessels by sensing the chemokins produced by lymphatic endothelial cells (chemoattraction) (36, 37).

Although the lymph node is filled with various immune cells, the microenvironment is immunosuppressive which is believed to occur prior to metastasis and the pre-metastatic niche emerges before cancer cells arrive (36). While migrating in the lymphatic vessel tumor cells continue to grow and survive. Cancer cells can escape the tumor draining lymph node through the efferent lymphatic vessel or invade the lymph node blood vasculature and further spread to other

lymph nodes and distant organs. Figure 2 demonstrate FDG uptake in a sentinel lymph node, and supplemental Figure 2 shows uptake in lymphatic channels and lymph nodes (38).

Metastases Through Vascular System

The metastatic cascade of hematogenous metastasis include developing a metastatic cell, establishment of a premetastatic niche, motility and invasion, intravasation, dissemination and transport, cellular arrest, vascular adhesion and extravasation and colonization (39).

Prior to leaving the tumor, cancer cells communicate with the other parts of the body through soluble factors to establish a pre-metastatic niche (40, 41). Stem cells are mobilized which arrive in the secondary microenvironment and prepare it before the arrival of cancer cells. Intravasation of detached cancer cells requires partial degradation of the extracelluar matrix and basement membrane underlying endothelial cells. During intravascular travel, some tumor cells evade immune attacks but some are killed by natural killer cells or hemodynamic sheer forces (Supplemental Figure 3) (39). Cancer cells evade the immune attacks by downregulating antigens and secreting substances to trick the immune system to recognize them as normal cells or to prevent immune cells directly killing them. By coating the cancer cells, platelets help them to gain physical and immune protection. Platelets and cancer cells also secrete substances to act on the monocytes and endothelial cells. Neutrophils can protect cancer cells from natural killer cells. The efficiency of metastasis increases if the tumor cells form emboli. For extravasation, tumor cells develop adhesion to the endothelial cells and penetrate the endothelium and the basement membrane with the help of metastasis-associated macrophages in the target tissue. After extravasation, tumor foci colonize in the new soil. Cancer cells modulate and restructure the new soil. Colonized cancer cells does not always grow as soon as they seed in the new soil. They can stay dormant and become

detectable in months to years. Various mechanisms are involved in cancer dormancy and reawakening.

Certain cancers seed in specific organs (organ tropism, seed and soil theory) which is regulated by multiple factors, such as interaction between tumor cells and the host microenvironment, circulation pattern, tumor-intrinsic factors, and organ-specific niches (39-42). The liver, lung, bone and brain are the most frequent sites of distant metastases. Common sites of hematogenous metastases vary among cancer types and subtypes.

Figure 3 demonstrate PET images of distant organ metastases from various cancers (43-45).

The bone is one of the most frequent site of tumor metastasis/spread from breast and prostate cancers and multiple myeloma. Multiple factors and expression of certain genes contribute to the homing of tumor cells to the bone. In osteolytic metastases and multiple myeloma bone lesions, the bone remodeling process is imbalanced, ephrin B2 and EphB4 expressions are downregulated (46). There is increased osteoclastic bone resorption driven by osteoclast-activating factors produced by the tumor or cells in the bone microenvironment. Tumor cells also produce osteoblast inhibitor factors. Myeloma cells produce growth factors that stimulate the growth of bone marrow stromal cells, which in turn produce osteoclast activating factors, such as IL-6, M-CSF, TNFa and RANKL. In osteoblastic metastases, there is new bone formation which is immature and of poor quality. Tumor cells secrete factors that induce osteoblastic proliferation and differentiation, such as TGF-β, VEGF, and FGF (46). In prostate cancer, prostate-specific antigen and other substances modify the bone microenvironment. Supplemental Figures 4, 5 and 6 demonstrates histopathology and PET images of osteolytic and osteoblastic bone metastases (47).

Liver is a common site for metastases from breast, lung and gastrointestinal malignancies. Hepatocytes directly interact with tumor cells to promote liver metastasis and also promote the formation of a pro-metastatic niche via secretion of various substances (42). Hepatic stellate and Kupffer cells are also involved in inducing/facilitating liver metastases. Lung is a common site for metastasis from breast, melanoma, and thyroid malignancies. Tumor-derived factors help tumor cell extravasation to the lung parenchyma. Neutrophils, chemokines, alveolar macrophages, and fibroblasts are involved in facilitating lung metastasis (42). Brain is a common metastatic site for lung cancer, breast cancer, and melanoma. Tumor cells produce certain substances to overcome the defense provided by the blood brain barrier. Astrocytes secrete many factors such as IL6, TGF-β, and IGF-1 to induce the growth of brain metastases (48). Figure 3 demonstrates rapid progression of brain metastasis.

Metastases Through Coelomic Cavities

Peritoneal spread of the tumor can occur due to direct rupture of the tumor into the peritoneal cavity, intraperitoneal seeding from ascites, or through hematogenous or lymphatic spread depending on the type of the primary tumor (49). Intraperitoneal seeding most commonly occurs from gastrointestinal and ovarian malignancies. During surgery or biopsy, secondary seeding may occur. Tumor cells adhere to the mesothelial lining of the peritoneum and invade the submesothelial connective tissues. Tumor cells initially grow focally in gravity-dependent recesses, in regions of stasis, pouches, paracolic gutters, umbilicus and subdiaphragmatic spaces but eventually diffusely involve both visceral and parietal peritoneum. Peritoneal carcinomatosis is usually associated with ascites. Supplemental Figure 7 demonstrates FDG PET/CT images of cases with peritoneal carcinomatosis.

Pleural spread of the tumor (pleural carcinomatosis) can develop as a direct extension of nearby cancer into the pleural space or through hematogenous or lymphangitic spread (50). Pleural tumor is usually associated with malignant pleural effusion. Pericardial spread of tumor may occur via lymphatic or hematogenous dissemination, local direct extension, or transvenous route by various tumors.

Krukenberg tumor is a rare metastatic signet ring cell tumor of the ovary with primary tumor in most of the cases is in stomach, colon, appendix and breast (particularly invasive lobular carcinoma). Mechanism could be via lymphogenous, hematogenous, and transcoelomic pathways (51).

Other Routes of Metastases

Lymphangitic Carcinomatosis

Lymphangitic carcinomatosis (LC) is diffuse infiltration and obstruction of parenchymal lymphatic channels by cancer cells with associated inflammation. The most common location is the lungs (pulmonary LC) and rarely it can occur in other organs. Pulmonary LC is usually seen in breast, lung, stomach, pancreas, ovary, and cervix cancers. The mechanism of LC is not well understood but can occur due to retrograde tumor spread into lymphatics through hilar/thoracic lymph nodes as a result of obstruction in lymphatic drainage, or antegrade movement of tumor cells from pleura to hilar lymph nodes through lymphatic vessels or hematogenous spread of metastatic disease to lung interstitium with subsequent lymphatic involvement or via tumor embolism (52). Histopathologically cancer cells are located within or around the lymphatics in the interstitium with edema and desmoplastic reaction. Figure 4 demonstrates PET/CT images of a case with pulmonary LC (53) .

Tumor Embolism and Tumor Thrombus

Tumor embolism can occur when cancer cells from solid tumors enter the circulation as individual or clusters of cells and lodge into various size of arteries or due to tumor fragments from intravascular tumor thrombus. Common sites of tumor embolism are aortic bifurcation, femoral, cerebral, pulmonary, renal and splenic arteries (54). Within the artery, tumor embolus may resolve, remain latent, or progress. Tumor embolism is more commonly seen with breast, lung, colon, stomach, kidney, ovarian and liver cancers. Tumor thrombus is extension of tumor into vessel, mainly into vein. Tumor thrombus is most frequently associated with renal cell, adrenal cortical, and hepatocellular carcinomas and Wilms tumor. Figure 5 demonstrates massive tumor emboli caused by intravascular tumor thrombus (55).

Tumor Spread Through Canalicules

Tumor can spread through canalicules such as bile, mammary, and nasolacrimal ducts, urinary tract, and airways. Cancer cells can also migrate along the basal side of endothelial cells without entering the lumen. Tumor spread through canalicules or ducts can be seen as a linear area of increased uptake on PET images. Figure 6 demonstrates PET images of tumor spread via a possible mammary duct in breast cancer and peri-biliary extension of tumor in cholangiocarcinoma (56).

Leptomeningeal Carcinomatosis

Leptomeningeal carcinomatosis is infiltration of cancer cells in the meningeal space surrounding the brain and spinal cord, which is more commonly seen in breast cancer, lung cancer, and melanomas. Cancer cells can reach the meningeal space by hematogenous spread, direct extension or drop metastases from metastatic or primary brain tumors and then disseminated by the cerebrospinal fluid flow in the meningeal space (57). It can also involve cranial nerves. Figure

7 (A) demonstrates drop metastasis into spinal medullary cavity (58). Metastases to cerebral ventricles are rare and could be caused by intracranial or extracranial tumors.

Perineural Tumor Invasion and Perineural Tumor Spread

Perineural tumor invasion is a histopathological (microscopic) finding of local infiltration of the nerves in the vicinity of the tumor whereas perineural tumor spread is macroscopic extension of the tumor along the nerve sheath. Studies have shown that perineural tumor growth is a molecularly mediated process and supportive cells within peripheral nerves interact with the cancer to promote invasion and dissemination of cancer cells along the nerves (59). Perineural tumor growth is more commonly seen in head and neck cancers (particularly facial, mandibular and maxillary nerves), but can also occur with various other cancers such as pancreas, prostate, and colorectal. MRI is a gold standard in detecting perineural tumor spread. Figure 7 (B) demonstrates PET/MR images of perineural tumor spread (60).

Conclusion

Biology of development and spread of cancer and role of PET imaging in Oncology were summarized and supported with various PET images demonstrating cancer spread patterns.

.

Compliance with Ethics Guidelines

No potential conflict of interest relevant to this article was reported.

References

1. American Cancer Society. Global Cancer Facts & Figures 4th Edition. Atlanta: American Cancer Society; 2018.
2. Steliarova-Foucher E, Colombet M, Ries LAG, et al. International incidence of childhood cancer, 2001-10: a population-based registry study. Lancet Oncol. 2017;18:719-731.
3. Ok CY, Woda B, Kurian E. The Pathology of Cancer. In: Pieters RS, Liebmann J, eds. Cancer Concepts: A Guidebook for the Non-Oncologist. Worcester, MA: University of Massachusetts Medical School; 2018. doi: 10.7191/cancer_concepts.1023.
4. Malarkey DE, Hoenerhoffl M, Maronpot RP. Carcinogenesis: Mechanisms and Manifestations. In Haschek and Rousseaux's Handbook of Toxicologic Pathology, Third Edition.http://dx.doi.org/10.1016/B978-0-12-415759-0.00005-4.
5. https://www.cancer.net/navigating-cancer-care/cancer-basics/genetics/genetics-cancer.
6. Welch DR, Hurst DR. Defining the Hallmarks of Metastasis. Cancer Res. 2019 15;79:3011-3027.
7. Welch DR. Tumor Heterogeneity- A 'Contemporary Concept' Founded on Historical Insights and Predictions. Cancer Res. 2016;76:4-6.
8. Hanahan D, Weinberg RA. Hallmarks of cancer: the next generation. Cell. 2011;144:646–74.
9. Martin TA, Ye L, Sanders AJ, et al. Cancer Invasion and Metastasis: Molecular and Cellular Perspective. In: Madame Curie Bioscience Database [Internet]. Austin (TX): Landes Bioscience; 2000-2013. Available from: https://www.ncbi.nlm.nih.gov/books/NBK164700/
10. Tarin D: The fallacy of epithelial mesenchymal transition in neoplasia. Cancer Res. 2005;65:5996-6001.
11. Mareel M, Oliveira MJ, Madani I. Cancer invasion and metastasis: interacting ecosystems. Virchows Arch. 2009;454:599-622.
12. Wu JS, Jiang J, Chen BJ, Wang K, Tang YL, Liang XH. Plasticity of cancer cell invasion: Patterns and mechanisms. Transl Oncol. 2021;14:100899.
13. Clark AG, Vignjevic DM. Modes of cancer cell invasion and the role of the microenvironment.

Curr. Opin. Cell Biol. 2015;36:13–22.

14. Lugano R, Ramachandran M, Dimberg A. Tumor angiogenesis: causes, consequences, challenges and opportunities. Cell Mol Life Sci. 2020;77:1745-1770.
15. Stacker SA, Williams SP, Karnezis T, Shayan R, Fox SB, Achen MG. Lymphangiogenesis and lymphatic vessel remodelling in cancer. Nat Rev Cancer. 2014;14:159-72.
16. Badawi RD, Shi H, Hu P, et al. First Human Imaging Studies with the EXPLORER Total-Body PET Scanner. J Nucl Med. 2019;60:299-303.
17. NCCN Clinical Practice Guidelines in Oncology (NCCN Guidelines). National Comprehensive Cancer Network. Version 4 2017-February.; 7: 2018.
18. Sarikaya I. Breast Cancer and PET Imaging. Nucl Med Rev Cent East Eur. 2021;24:16-26.
19. MacMahon H, Naidich DP, Goo JM, et al. Guidelines for Management of Incidental Pulmonary Nodules Detected on CT Images: From the Fleischner Society 2017. Radiology. 2017;284:228-243.
20. Taïeb D, Hicks RJ, Hindié E, et al. European Association of Nuclear Medicine Practice Guideline/Society of Nuclear Medicine and Molecular Imaging Procedure Standard 2019 for radionuclide imaging of phaeochromocytoma and paraganglioma. Eur J Nucl Med Mol Imaging. 2019;46:2112-2137.
21. Morigi JJ, Stricker PD, Leeuwen PJV, et al. Prospective Comparison of 18F-Fluoromethylcholine Versus 68Ga-PSMA PET/CT in Prostate Cancer Patients Who Have Rising PSA After Curative Treatment and Are Being Considered for Targeted Therapy. J Nucl Med. 2015;56:1185-90.
22. Calais J, Ceci F, Eiber M, et al. ^{18}F-fluciclovine PET-CT and ^{68}Ga-PSMA-11 PET-CT in patients with early biochemical recurrence after prostatectomy: a prospective, single-centre, single-arm, comparative imaging trial. Lancet Oncol. 2019; 20: 1286–1294.
23. Giovanella L, Treglia G, Iakovou I, Mihailovic J, Verburg FA, Luster M. EANM practice guideline for PET/CT imaging in medullary thyroid carcinoma. Eur J Nucl Med Mol Imaging. 2020;47:61-77.
24. Hicks RJ, Roselt PJ, Kallur KG, Tothill RW, Mileshkin L. FAPI PET/CT: Will It End the

Hegemony of ^{18}F-FDG in Oncology? J Nucl Med. 2021;62:296-302.

25. Sarikaya I, Sarikaya A. Assessing PET Parameters in Oncologic ^{18}F-FDG Studies. J Nucl Med Technol. 2020;48:278-282.
26. Wahl RL, Jacene H, Kasamon Y, et al. From RECIST to PERCIST: Evolving Considerations for PET Response Criteria in Solid Tumors. JNM. 2009; 50(Suppl_1), doi: 10.2967/jnumed.108.057307.
27. Carson R, Berg E, Badawi R, et al. Design of the NeuroEXPLORER, a next-generation ultra-high performance human brain PET imager. JNM 2021;62 (supplement 1):1120.
28. Schierz JH, Sarikaya I, Wollina U, Unger L, Sarikaya A. Immune checkpoint inhibitor related adverse effects and FDG PET/CT findings. J Nucl Med Technol. 2021:jnmt.121.262151. doi: 10.2967/jnmt.121.262151.
29. Sarikaya I, Sarikaya A, Sharma P. Assessing the Effect of Various Blood Glucose Levels on ^{18}F-FDG Activity in the Brain, Liver, and Blood Pool. J Nucl Med Technol. 2019;47:313-318.
30. Zasadny KR, Wahl RL. Standardized uptake values of normal tissues at PET with 2-[fluorine 18]fluoro-2-deoxy-D-glucose: variations with body weight and a method for correction. Radiology. 1993;189:847–850.
31. Sarikaya I, Albatineh AN, Sarikaya A. Revisiting Weight-Normalized SUV and Lean-Body-Mass-Normalized SUV in PET Studies. J Nucl Med Technol. 2020;48:163-167.
32. Im HJ, Bradshaw T, Solaiyappan M, Cho SY. Current Methods to Define Metabolic Tumor Volume in Positron Emission Tomography: Which One is Better? Nucl Med Mol Imaging. 2018;52:5-15.
33. Sarikaya I, Sarikaya A. PET/CT Image Artifacts Caused by the Arms. J Nucl Med Technol. 2021;49:19-22.
34. Sarikaya I, Elgazzar AH, Sarikaya A, Alfeeli M. Normal bone and soft tissue distribution of fluorine-18-sodium fluoride and artifacts on 18F-NaF PET/CT bone scan: a pictorial review. Nucl Med Commun. 2017;38:810-819.
35. Sarikaya I, Yeung HW, Erdi Y, Larson SM. Respiratory artefact causing malpositioning of

liver dome lesion in right lower lung. Clin Nucl Med. 2003;28:943-4.

36. Zhou H, Lei PJ, Padera TP. Progression of Metastasis through Lymphatic System. Cells. 2021;10:627.

37. Borsig L, Wolf MJ, Roblek M, Lorentzen , Heikenwalder H. Inflammatory chemokines and metastasis–tracing the accessory.Oncogene 2014;33:217–3224.

38. Sarikaya I, Sarikaya A. Assessing ^{18}F-FDG Uptake in the Sentinel Lymph Node in Breast Cancer. J Nucl Med Technol. 2019;47:149-153.

39. Lambert AW, Pattabiraman DR, Weinberg RA. Emerging Biological Principles of Metastasis. Cell. 2017;168:670-691.

40. Psaila B, Lyden D. The metastatic niche: adapting the foreign soil. Nat Rev Cancer 2009;9:285-93.

41. Kaplan RN, Rafii S, Lyden D. Preparing the "soil": the premetastatic niche. Cancer Res 2006;66:11089–93.

42. Gao Y, Bado I, Wang H, et al. Metastasis Organotropism: Redefining the Congenial Soil. Dev Cell. 2019;49:375-391.

43. Rust E, Hubele F, Marzano E, et al. Nuclear medicine imaging of gastro-entero-pancreatic neuroendocrine tumors. The key role of cellular differentiation and tumor grade: from theory to clinical practice. Cancer Imaging. 2012;12:173-84.

44. Giesel FL, Kratochwil C, Lindner T, et al. ^{68}Ga-FAPI PET/CT: Biodistribution and Preliminary Dosimetry Estimate of 2 DOTA-Containing FAP-Targeting Agents in Patients with Various Cancers. J Nucl Med. 2019;60:386-392.

45. Ulaner GA, Jhaveri K, Chandarlapaty S, et al. Head-to-Head Evaluation of ^{18}F-FES and ^{18}F-FDG PET/CT in Metastatic Invasive Lobular Breast Cancer. J Nucl Med. 2021;62:326-331.

46. David Roodman G, Silbermann R. Mechanisms of osteolytic and osteoblastic skeletal lesions. Bonekey Rep. 2015;28;4:753.

47. Roudier MP, Morrissey C, True LD, et al. Histopathological assessment of prostate cancer bone osteoblastic metastases. J Urol. 2008;180:1154-60.

48. Valiente M, Ahluwalia MS, Boire A, et al. The evolving landscape of brain metastasis. Trends Cancer. 2018;4:176–196.

49. Levy AD, Shaw JC, Sobin LH. Secondary tumors and tumorlike lesions of the peritoneal cavity: imaging features with pathologic correlation. Radiographics. 2009;29:347-73.

50. Agalioti T, Giannou AD, Stathopoulos GT. Pleural involvement in lung cancer. J Thorac Dis. 2015;7:1021-30.

51. Wu F, Zhao X, Mi B, et al. Clinical characteristics and prognostic analysis of Krukenberg tumor. Mol Clin Oncol. 2015;3:1323-1328.

52. Biswas A, Sriram PS. Getting the whole picture: lymphangitic carcinomatosis. Am J Med. 2015;128:837-40.

53. Tang VD, Campbell P, Pattison DA. Lymphangitic Carcinomatosis From Prostate Cancer Identified With Gallium-68 Prostate-specific Membrane Antigen Positron Emission Tomography Imaging. Urology. 2018;114:e1-e2.

54. Azevedo AS, Follain G, Patthabhiraman S, Harlepp S, Goetz JG. Metastasis of circulating tumor cells: favorable soil or suitable biomechanics, or both? Cell Adh Migr. 2015;9:345-56.

55. Ogawa Y, Abe K, Hata K, Yamamoto T, Sakai S. A case of pulmonary tumor embolism diagnosed with respiratory distress immediately after FDG-PET/CT scan. Radiol Case Rep. 2021;16:718-722.

56. Mar WA, Shon AM, Lu Y, et al. Imaging spectrum of cholangiocarcinoma: role in diagnosis, staging, and posttreatment evaluation. Abdom Radiol (NY). 201641:553-67.

57. Kokkoris CP. Leptomeningeal carcinomatosis. How does cancer reach the pia-arachnoid? Cancer. 1983;51:154–160.

58. Jain TK, Basher RK, Sood A, Mittal BR, Prakash G, Bhatia A. ^{18}F-FDG PET/CT Finding of Drop Metastases from Germ Cell Tumor of Pineal Gland. J Nucl Med Technol. 2017;45:114-115.

59. Bakst RL, Glastonbury CM, Parvathaneni U, Katabi N, Hu KS, Yom SS. Perineural Invasion and Perineural Tumor Spread in Head and Neck Cancer. Int J Radiat Oncol Biol Phys. 2019;103:1109-1124.

60. Paes FM, Singer AD, Checkver AN, Palmquist RA, De La Vega G, Sidani C. Perineural spread in head and neck malignancies: clinical significance and evaluation with 18F-FDG PET/CT. Radiographics. 2013;33:1717-36.

Figure Legends

Figure 1

Development of parotid cancer. Selected serial FDG PET MIP images of the head and neck in a patient with breast cancer. Mild focal uptake in the left parotid gland in 2017 becomes larger and more hypermetabolic in 2020 (arrows). Histopathology showed mucoepithelial cancer. There is no abnormal uptake in the left parotid in 2016 which could be due to lack of tumor at that time or microscopic/small volume tumor which is below PET resolution.

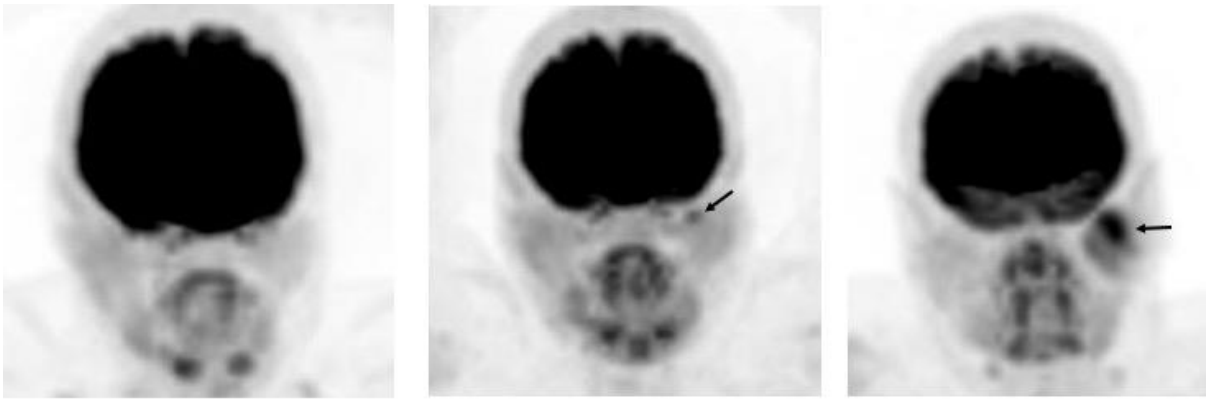

Figure 2

Early metastasis in the sentinel lymph node (SLN). SLN SPECT/CT and FDG PET/CT images (selected transaxial) of a patient with newly diagnosed bilateral invasive lobular breast cancer. SPECT/CT image shows the right SLN (arrow). FDG PET/CT image shows mild uptake in the right SLN (arrow) (biopsy: metastasis). FDG uptake in left axillary lymph node is also due to metastasis. Reprinted with permission from SNMMI, altered and colored (38).

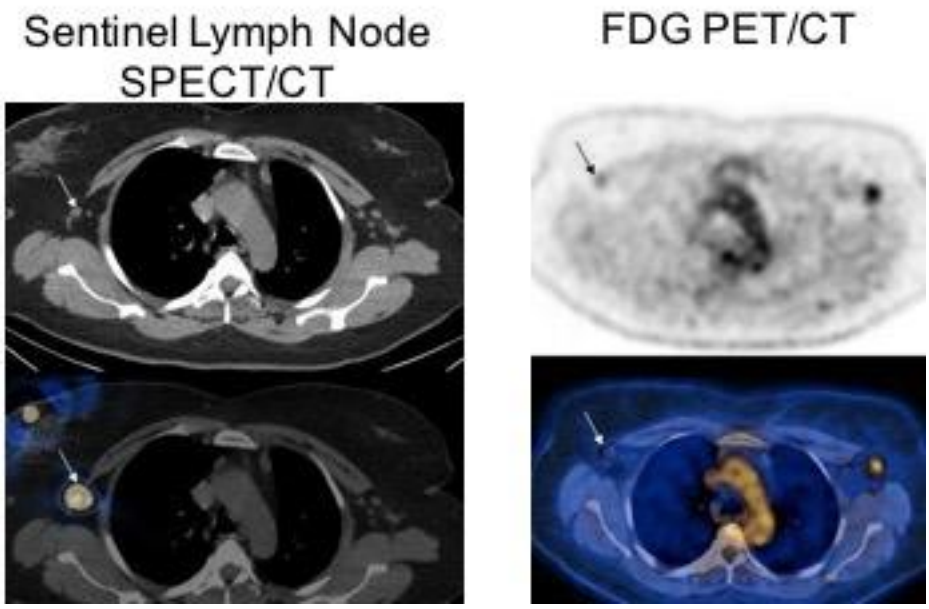

Figure 3

18F-FDG PET images of various cancers and metastases (Top). A- Right breast cancer (invasive ductal) with multiple metastases in the bones, liver, right adrenal and right axillary lymph nodes. B- Right breast cancer (poorly differentiated neuroendocrine tumor) with multiple metastases in the lungs, liver and right axillary lymph nodes. C- Colon cancer in the splenic flexure (arrow) with a large metastasis in the liver. D-Rapid progression of brain metastasis in a case with right lung cancer. Whole body image demonstrates a hypermetabolic right lung tumor. On initial scan there is mild focal uptake in the tail of right putamen (PET/CT fusion, top image, arrow). PET image 3 mo later (no treatment) shows significant increase in size and metabolic activity of the metastatic focus in the brain (PET/CT fusion, bottom image, arrow). PET images with various other radiotracers (bottom row). A- 68Ga-DOTANOC PET image of a patient with small bowel carcinoid. Primary tumor (left arrow) and multiple mesenteric metastases, all with high SSR binding (arrow). B- 68Ga-PSMA-11 PET image in a patient with prostate cancer shows diffuse bone and multiple abdominal and pelvic lymph node metastases. C-18F-FDOPA PET image in a patient with history of well-differentiated ileal neuroendocrine tumor which is surgically treated shows intense uptake in multiple large hepatic metastases (Reprinted with permission from Springer Nature and altered) (43). D- 68Ga-FAPI PET in a patient with NSCLC shows intense uptake in the primary tumor and metastatic foci in the mediastinum and bilateral supraclavicular regions (Reprinted with permission from SNMMI and altered) (44). E-18F-fluoroestradiol PET in a patient with invasive lobular breast cancer shows extensive bone and bone marrow involvement with high ER binding (Reprinted with permission from SNMMI and altered) (45).

FDG

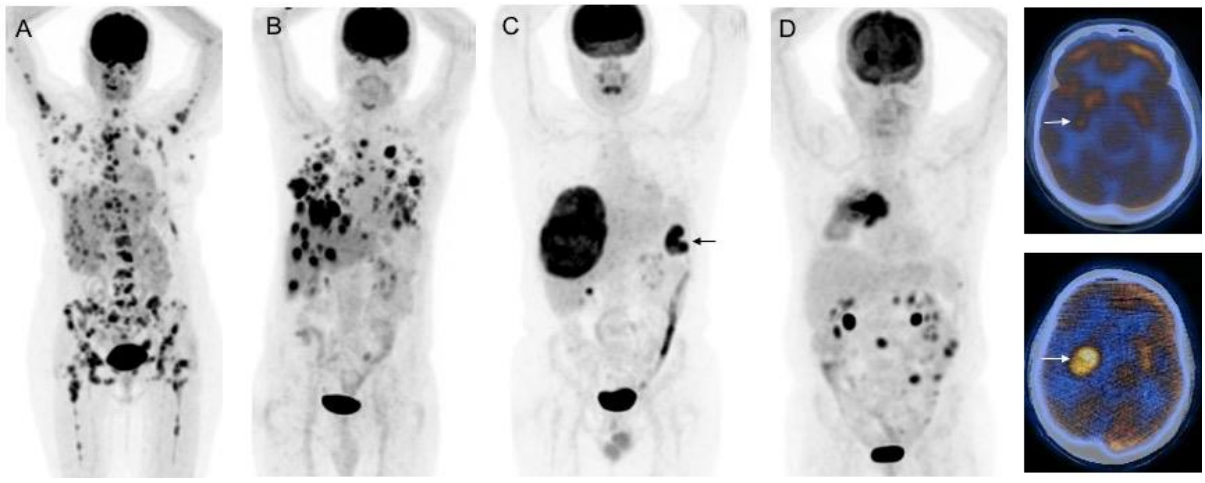

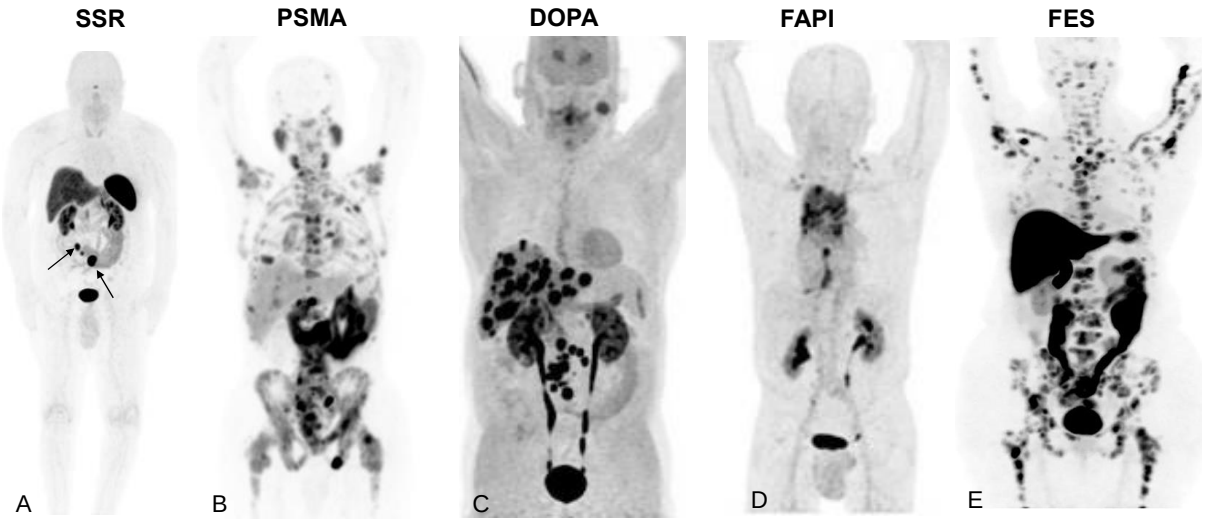

Figure 4

Pulmonary lymphangitic carcinomatosis in a case with prostate cancer. Whole body PET, selected transaxial CT and 68Ga-PSMA ligand images show widespread thickening of the interlobular septae and diffusely increased radiotracer uptake (Reprinted with permission from Elsevier and altered) (53).

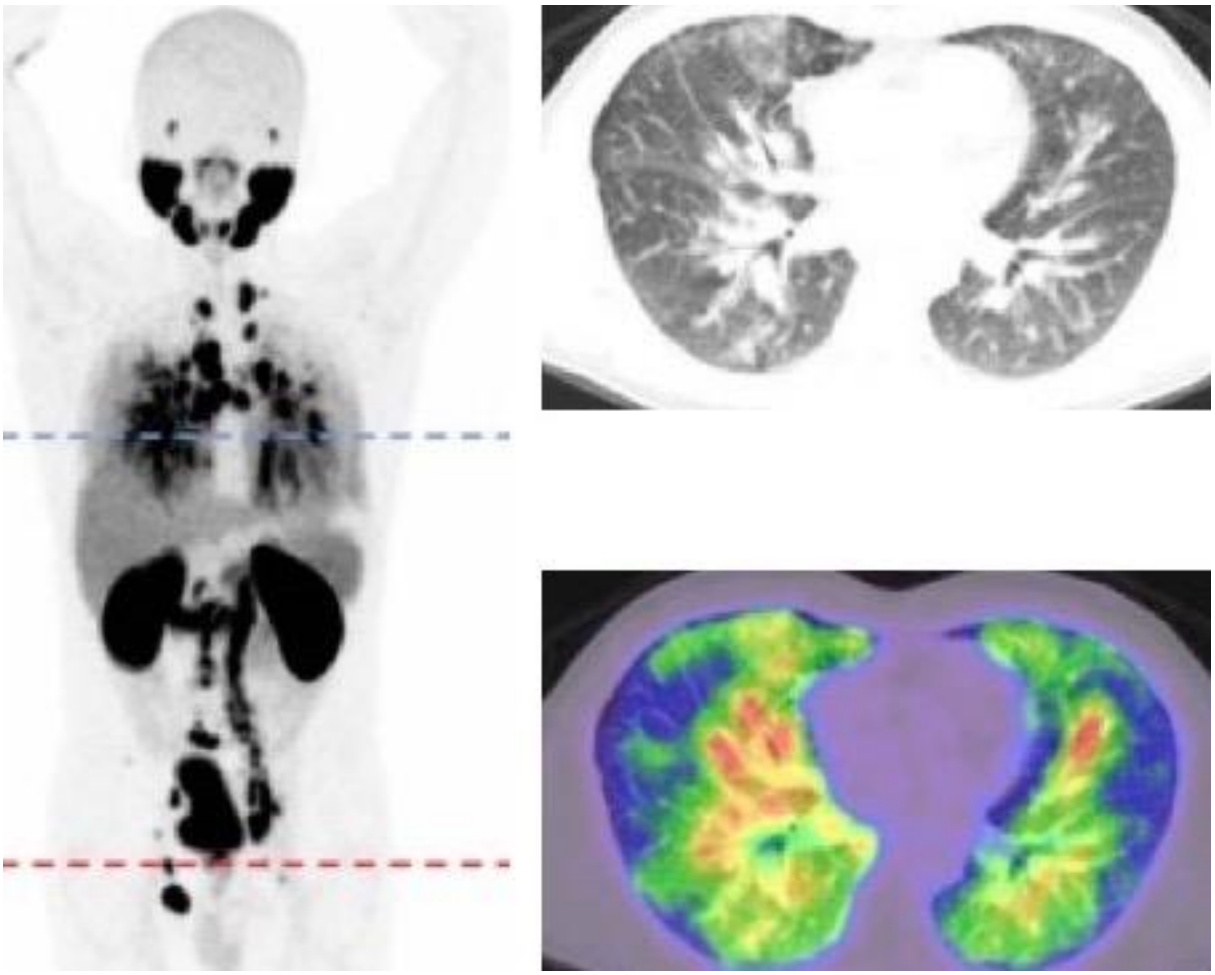

Figure 5

Massive pulmonary tumor emboli from intravascular tumor thrombus in a case with renal cell carcinoma. PET/CT fusion and MIP images demonstrate FDG accumulation in the left renal tumor which was continuously observed in the left renal vein and extended into an infradiaphragmatic IVC and the left ovarian vein (C, D, and E, black arrows). FDG uptake in the left distal pulmonary artery and bilateral branches (A and E, white arrowheads) and right atrial cavity (B and E, white arrows) were also presented (Reprinted with permission from Elsevier) (55).

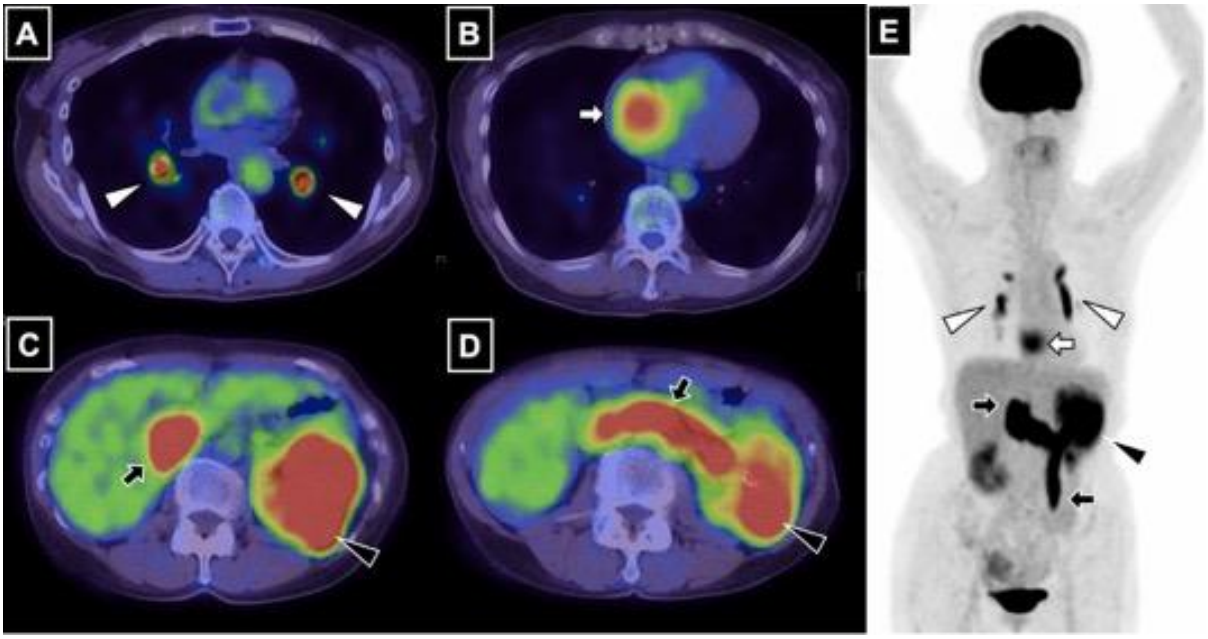

Figure 6

A-Selected transaxial CT, FDG PET and PET/CT fusion images in a case with tubular breast cancer show a hypermetabolic primary tumor (arrow) and either a mammary duct extending to nipple or a lymphatic channel extending to Sappey's plexus with mild activity representing intraluminal tumor uptake (arrow heads). B-Infiltrating perihilar cholangiocarcinoma with peribiliary extension. Coronal T1-weighted contrast-enhanced MR image shows enhancing tumor of the confluence of the right ducts (white arrow), intrahepatic ductal dilation and enhancing right peribiliary extension (black arrow). FDG PET MIP image shows an FDG avid perihilar tumor (white arrow) with peribiliary extension (black arrow) (Reprinted with permission from Springer and altered) (56).

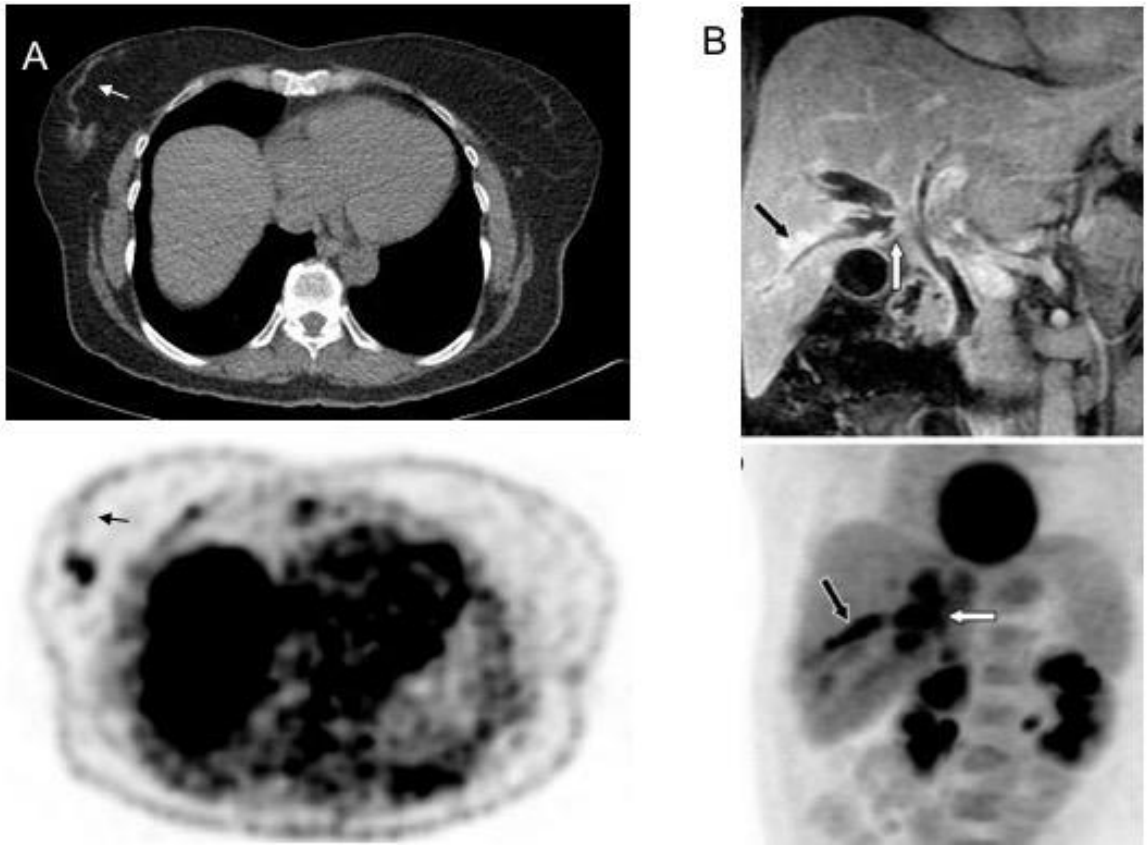

Figure 7

A- Drop Metastases in the spinal canal from germ cell tumor of pineal gland. Head CT and FDG PET show avidly enhancing hypermetabolic nodular lesion in the pineal gland (arrows). Selected sagittal CT and FDG PET/CT fusion images show increased uptake in ill-defined densities in spinal canal extending from L1 to L5 (arrows) (Reprinted with permission from SNMMI and altered) (58). B- Perineural tumor spread along V3 (mandibular) nerve. Coronal FDG PET/CT and contrast-enhanced T1-weighted fat-saturated MR images show intense FDG accumulation and abnormal enhancement along V3 (arrowheads) (Reprinted with permission from RSNA altered) (60).

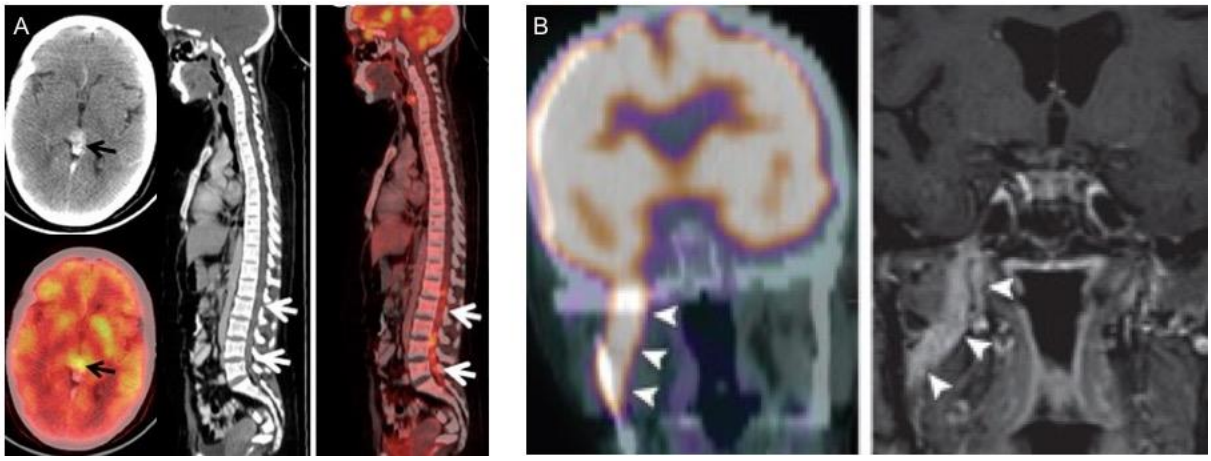

Table 1- Common and uncommon oncologic PET radiotracers with uptake mechanisms.

PET Study	Measures/Targets	Mechanism of Uptake in Cancer	Main Indications/Studied	Availability
FDG	Glucose metabolism (indirect)	cellular uptake via GLUT1 and phosphorylation by hexokinase	Various cancers	Widely, routine
SSTA	Somatostatin receptors (SSR)	binds mainly to SSR-2, and in a lesser degree to SSR3 and SSR5	Well- and moderately-differentiated NETs	Increasing
PSMA	Cellular PSMA	binds to cellular PSMA and internalize	Prostate cancer	Increasing
NaF	Osteoblastic activity	exchange of 18F-ions with hydroxyl ions on the surface of the hydroxyapatite to form fluoroapatite	Bone metastases from various cancers	Increasing
FLT	Cellular proliferation (indirect)	phosphorylated by thymidine kinase (not incorporated into DNA)	Various cancers; NSCLC, lymphomas	Limited
FET	AA uptake by transporters	enters the cells by L-type amino acid transporter (LAT-1)	Brain tumors, particularly gliomas	Limited
MET	AA uptake and protein synthesis	enters the cells by LAT1 and is involved in the synthesis of proteins and phospholipids	Brain tumors, particularly gliomas	Limited
FLUC	AA uptake by transporters	enter the cells by amino acid transporter ASCT2 and LAT1	Prostate cancer	Limited
FDOPA	DOPA transport, storage, and metabolism	enters the NE cells by LAT1, converted to dopamine by AA decarboxylase and trapped in vesicles via VMAT	NETs, Pheo, Neuroblastoma, PG, Gliomas	Limited
Choline	Cell membrane synthesis/Cellular proliferation	phosphorylated by choline kinase to phosphocholine, and converted to phosphatidylcholine	Prostate cancer	Limited
Acetate	Cellular proliferation	incorporates into cellular membrane	HCC (well-diff) , Renal cancers	Limited
FAPI	Cancer associated fibroblasts (CAFs)	binds to fibroblast-activation-protein (FAP) on CAFs	Various cancers	Limited
FES	Estrogen receptor (ER)	binds to ER	Breast cancer, Ovarian cancer	Limited
HER2	Human epidermal growth factor (HER2)	binds to HER2	Breast cancer	Limited
FDHT	Androgen receptor (AR)	binds to AR	Prostate cancer	Limited
Iodine	Iodine metabolism	taken up by thyroid follicular cells via Na+/I- symporter, oxidixed by thyroid peroxidase, stays in the colloid or leave as thyroid hormones	Well-differentiated thyroid cancer	Limited

MIBG	Norepinephrine (NE) transporter	taken up by the sympathicomedullary tissue via the NE transporter (uptake-1 system), stored in neurosecretory granules	Pheo, neuroblastoma, PG	Limited
FMISO	Hypoxia	nitro-group undergoes reduction in hypoxia, form highly reactive oxygen radicals, binds to intracellular macromolecules	Various cancers, particularly brain and HN	Limited
ATSM	Hypoxia	possible mechanisms: accumulation in regions with higher CD133+ expression, and activation of the hypoxia inducible factor 1	Various cancers, particularly brain and HN	Limited
Folate	Folate receptor-alpha (FR-alpha)	binds to FR-alpha	Various cancers	Limited
Pentixafor	CXC motif chemokine receptor 4	binds to CXC motif chemokine receptor 4	Various cancers	Limited
Lactate	Lactate metabolism	oxidative phosphorylation	Various cancers	Limited
Immuno PET	Tumor associated antigens (TAAs)	Monoclonal antibodies bind to TAAs	Various Cancers	Limited

FDG: 18F-fluorodeoxyglucose, SSTA: Somatostatin analog, 68Ga-DOTA-Peptides (DOTATATE, DOTATOC, DOTANOC), PSMA: 68Ga-PSMA ligand, NaF: 18F-Sodium fluoride, FLT:18F-fluorothymidine, FET:18F-fluoroethyltyrosine, MET:11C-Methionine, FLUC: ^{18}F-*fluciclovine*, *FDOPA:18*F-DOPA, Choline:11C-choline and 18F-fluorocholine, Acetate: 11C-acetate, FAPI: ^{68}Ga-*FAPI*, *FES:18*F-fluoroestradiol, HER2: 89Zr-trastuzumab, FDHT:^{18}F-fluorodihydrotestosterone, Iodine:124Iodine, MIBG: 124I-metaiodobenzylguanidine, FMISO:18F-FMISO, ATSM: ^{64}Cu-*ATSM*, *Folate:* Various radiotracers, Pentixafor: 68Ga-*Pentixafor. PG: Paraganglioma. NET: Neurendocrine tumor. HN: Head and neck.*

Supplemental Figures

Supplemental Figure 1

A large markedly hypermetabolic left breast tumor (IDC) invading the skin, nipple, areola and pectoralis muscles with loss of fat plane on CT (arrows) (selected transaxial CT and FDG PET/CT fusion images). A hyermetabolic focus is also seen in the right lung and multiple other foci/metastases in the lymph nodes, bones and both lungs (not shown).

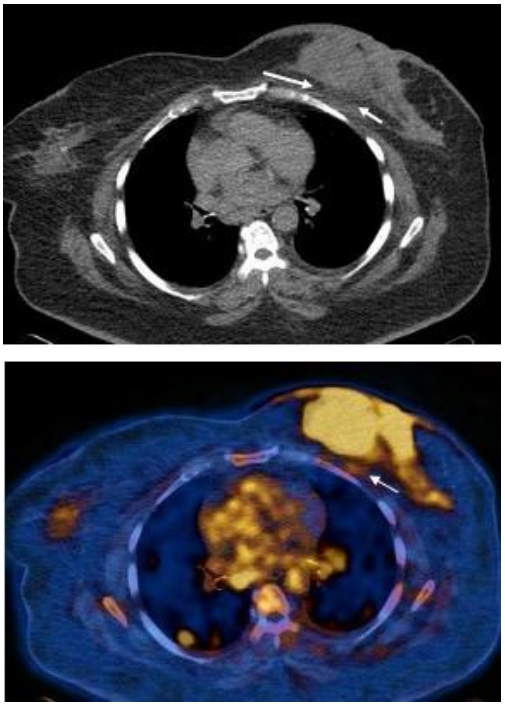

Supplemental Figure 2

Tumor uptake in the lymphatic channels. Selected transaxial CT, FDG PET and PET/CT fusion images in two cases with newly diagnosed breast cancer. A- Images show the hypermetabolic primary tumor in the right breast (arrow) invading the skin/nipple, and a lymphatic channel with mild linear uptake (arrows) extending from primary to a secondary focus (arrow) which is larger and more hypermetabolic than the primary focus. B- Images show the hypermetabolic primary tumor in the left breast (arrow) and a lymphatic channel arising from the tumor directing towards the axilla with mild linear uptake (arrow) and uptake in the left axillary lymph node. C- FDG PET images showing lymph node metastases. Multifocal left breast tumor (IDC) with multiple lymph node metastases in the left axilla, subclavicular and supraclavicular regions.

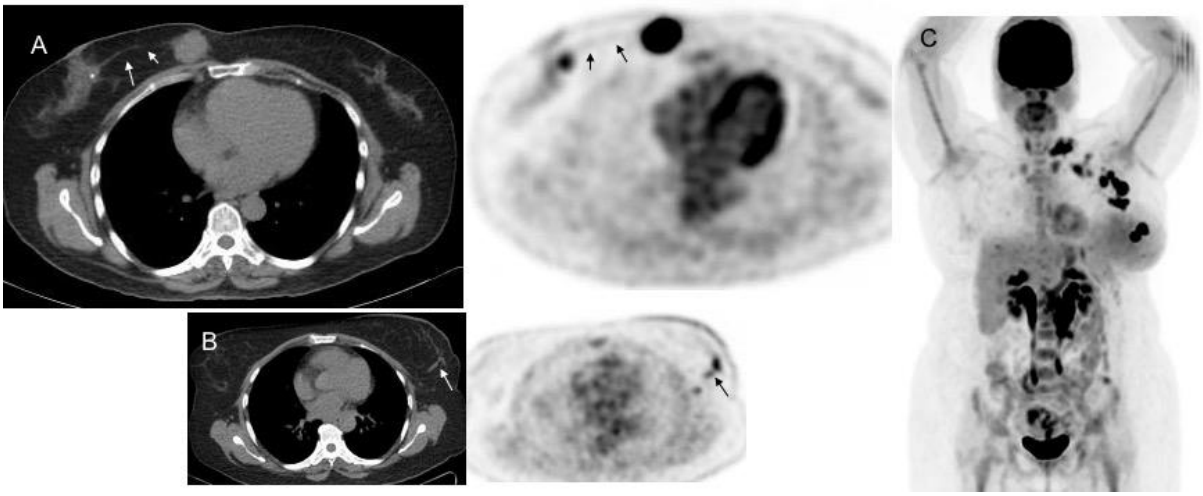

Supplemental Figure 3

Cancer cells escaping from the primary tumor, traveling in the circulation, interacting with the various cells and substances in the circulation, and entering into new soil (Reprinted with permission from Elsevier) (39).

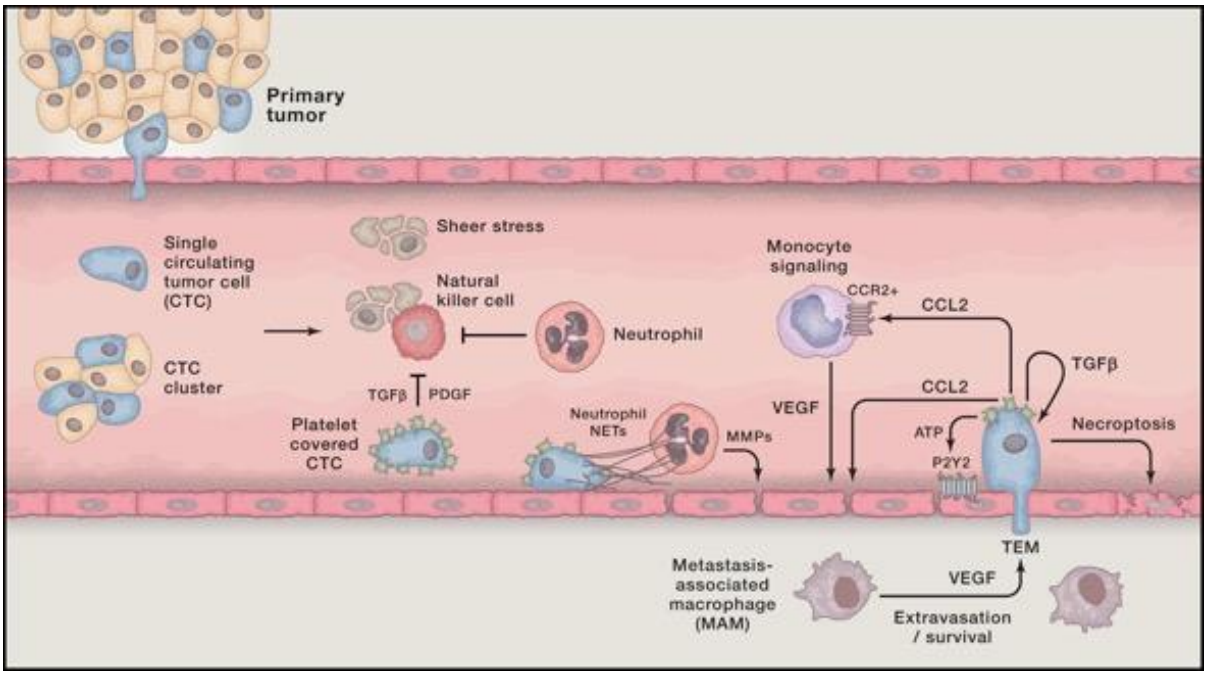

Supplemental Figure 4

Spectrum of histological patterns observed in prostate cancer bone metastases from one patient: A- Osteodense biopsy and B- Osteopenic biopsy taken from two different anatomical sites in the same patient. In all biopsies, bone marrow is entirely filled with prostate cancer cells. Magnification 5x. (Reprinted with permission from Elsevier. Image altered (47).

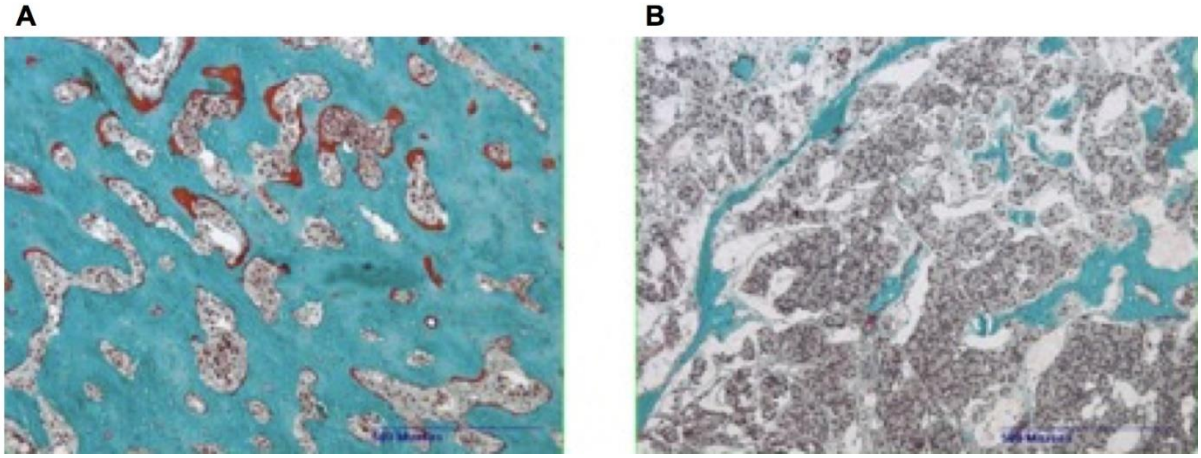

Supplemental Figure 5

Lytic bone metastases. Selected transaxial CT, FDG PET and PET/CT fusion images. A- In a case with breast cancer, CT shows only minimal lytic changes in the vertebral cortex laterally on the left (arrow) but FDG PET shows multiple foci of markedly increased metabolic activity in the vertebra. B-In a case with breast cancer, CT shows significant lytic and destructive changes in the vertebral body and PET shows markedly increased metabolic activity which is heterogeneous. C-In a case with multiple myeloma, FDG PET shows an active hypermetabolic intramedullary lesion which invades the bone and causes a lytic lesion as seen on CT image. FDG PET has higher sensitivity in detecting osteolytic bone metastases than osteoblastic ones. This is mainly due to higher cancer cell density in lytic lesions than osteblastic lesions and also lytic metastases to arise from more aggressive primary tumors which are highly FDG avid.

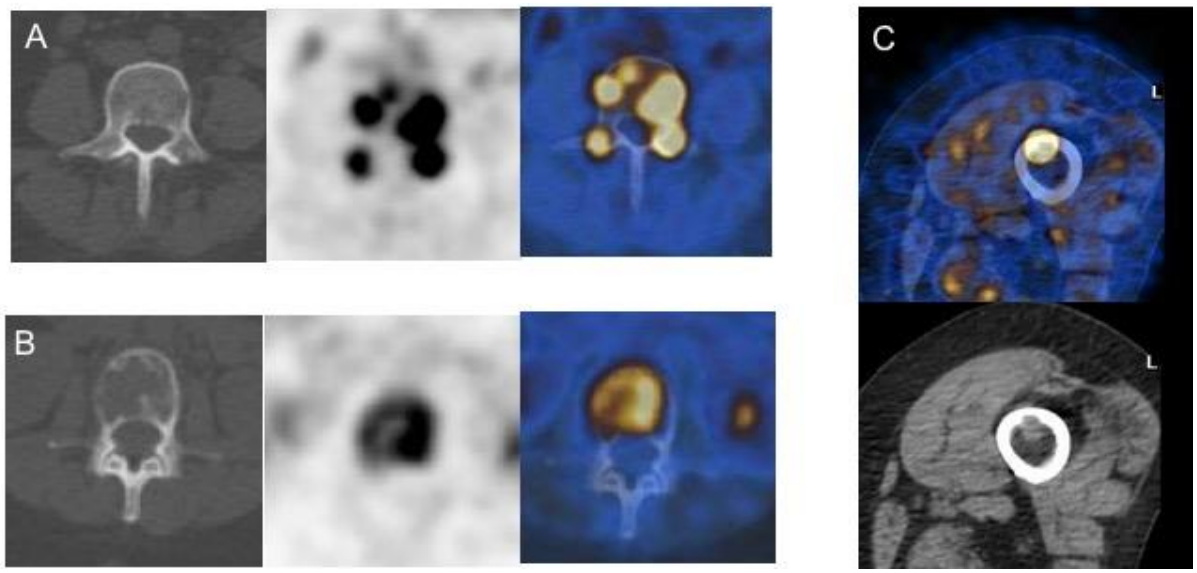

Supplemental Figure 6

A-Diffuse osteoblastic metastases in a case with prostate cancer. NaF PET MIP and sagittal CT, PET and PET/CT fusion images show multiple sclerotic foci in the axial bones seen on CT (only spine shown) and diffusely and heterogeneously increased osteoblastic metabolic activity in the axial bones. B-Mixed lytic-sclerotic lesions in a case with breast cancer. CT shows lytic and sclerotic changes in the left posterior iliac bone. NaF PET shows increased uptake corresponding to sclerotic changes and FDG PET shows increased uptake in the anterior iliac region and focal uptake in focal lytic area in posterior iliac. FDG PET has low sensitivity in detecting osteoblastic metastases because the cancer cell density in the tumor tissue is low due to new bone formation and also they usually arise from tumors which are less aggressive or have low FDG avidity.

Supplemental Figure 7

Peritoneal carcinomatosis in two cases. FDG PET MIP, and selected transaxial CT, PET and PET/CT images of the abdomen. A- There is omental thickening/nodularity and diffusely increased uptake (omental caking) in a case with endometrial cancer. B- There is ascites with faint uptake and mild diffusely increased uptake along the parietal peritoneum in a case with breast cancer. Uptake in the region of the bowel loops could be from visceral peritoneal uptake versus physiological bowel activity.